New advanced SiC-based composite materials for use in highly oxidizing environments: synthesis of $SiC/IrSi_3$

Antonio Camarano[1], Javier Narciso[1], Donatella Giuranno[2,3*]

Antonio Daniel Camarano[1]: antoniodaniel.camarano@ua.es
Javier Narciso[1]: narciso@ua.es
Donatella Giuranno[2,3*], corresponding author email: donatella.giuranno@ge.icmate.cnr.it,

Affiliations:

[1] Instituto Universitario de Materiales de Alicante (IUMA), Universidad de Alicante, Apdo. 99, Alicante, 03080, Spain
[2]Institute of Condensed Matter Chemistry and Energy Technologies (ICMATE), National Research Council of Italy (CNR),Via De Marini 6, Genoa, 16149, Italy
[3]Foundry Research Institute, Zakopiańska 73 Str., 30-418 Krakow, Poland

Abstract

Currently, MMCs with SiC as reinforcement emerge as ideal candidates for long-term stable devices withstanding high temperatures and harsh operating environments which are typical for many industrial sectors, such as energy, aerospace, electronics, cataysis, etc. However, the costly manufacture of such composites is the major restraint to make them marketable.

In this paper, highly-dense, nearly-shaped $SiC/IrSi_3$ composites effortless produced at T = 1250°C under a vacuum by reactive melt infiltration of liquid Si-62wt%Ir eutectic alloy into bimodal SiC_p-C porous preforms, are presented. The replacement of unreacted detrimental Si by a tougher and less oxidizing intermetallic phase ($IrSi_3$) was successfully obtained.

1. Introduction

The future of composite materials is extremely bright. In particular, advanced composites will dominate in almost any industrial sector. Aerospace industry and energy production are just two of the many market segments that will see a large increase in the use of ad-hoc designed materials, with outstanding performance and long-term stability in operating at high temperature and oxidizing environments.

To date, metal-matrix (MMCs) and ceramic-matrix composite materials (CMCs), in particular SiC-based composites, meet the aforementioned requirements [1, 2], because the combination of

their remarkable features, such as excellent thermo-mechanical properties, high wear resistance and remarkable chemical stability in corrosive-oxidizing environments [3, 4].

Whether SiC is the matrix or present as reinforcing phase, it is a refractory material with excellent properties strictly related to the strong covalent bond between Si and C. However, a so strong covalent bond also represents an inconvenient in the SiC-synthesis and production. Indeed, owing to low self-diffusion coefficient, by using conventional sintering process, it is very difficult to obtain compact or at least highly dense SiC (reduced porosity). Moreover, sintered SiC is a costly product manufactured in limited simple geometries cause the severe operating conditions required (> 1800°C, 10-40 MPa) [5-9]. In order to solve this technological problem, alternative processes have been proposed and developed such as reactive infiltration [10-12] and chemical vapor infiltration (CVI) [13-15]. In particular, the reactive infiltration of carbon (C) or SiC-based preforms by liquid silicon (Si), named Reaction Bonded Silicon Carbide (RBSC), allows to fabricate highly-dense, shaped and cost-less SiC at lower temperatures (1450–1600°C) than conventional ones, and without applying any external pressure or using additives [16–19]. Despite these advantages, the main drawback of these products is the presence of unreacted Si (5-25vol%) compromising the overall mechanical performance of the composite. The replacement of such metal phase with intermetallic compounds (silicides) like $MoSi_2$ [20], WSi_2 [21], $CoSi_2$ [22,23] or $ZrSi_2$ [24], has recently gained attention in developing structural composites as candidates for extremely high-temperature applications. As demonstrated, the mentioned composites, easily manufactured by reactive infiltration, were exhibiting a good thermo-mechanical performance and microstructural long-term stability combined with oxidation resistance [25].

In this context, even if limited to some “niche” applications, Iridium (Ir) and Ir-silicides arise as new and suitable alternative constituents worthy to be investigated as Si-replacement phase in RBSC process. In fact, Ir exhibits a unique set of properties almost meeting the key requirements in a wide range of highly demanding applications [26], such as the high melting temperature (2446°C) [27], high specific strength at high temperature, remarkable oxidation and corrosion resistance. To now, Ir is already used in catalysis [28,29], to manufacture high temperature crucibles, for dental implants and jewellery, for sensors [30] and electronic devices working at high temperatures (dimensionally stable anodes) [31]. Ir is used also as hardening agent for other metals, (such as Pt [32]) and multicomponent alloys [33]. As reported by [34, 35], in its massive state, Ir is not soluble in acids, salts, does not reacts with C to form carbides, shows negligible C-solubility and it is virtually impenetrable by oxygen up to T = 2370°C. Therefore, Ir is successfully used as coating material for various substrates acting as a chemically stable oxygen

diffusion barrier even at high temperature [36-39]. Similarly, Ir-Si system and Ir-silicides, show improved thermo-mechanical properties [40] and consequently, enhanced oxidation resistance [41,42]. Additionally, going back to composites, the Si, Ir and SiC coefficients of thermal expansion (CTE) [43-45], are almost comparable. The thermal-compatibility among the constituent phases is crucial in predicting, in a composite material, catastrophic failure caused by thermal expansion mismatch.

In this paper, the successful synthesis of highly dense SiC/$IrSi_3$ composite materials by reactive infiltration of liquid Si-62wt%Ir eutectic alloy (Si-19.5at%Ir) [46] into bimodal SiC_p-C preform is presented as main achievement. In particular, SiC/$IrSi_3$ were cost-less obtained at T = 1250°C and under a vacuum. In addition, a careful analysis of infiltration kinetics as a function of the actual operating conditions, interfacial phenomena observed and related microstructure development was performed. In order to evaluate the viability of the selected route, the results obtained are compared with those of produced SiC/Si composite material using the same procedure.

2. Experimental details

2.1. Materials

The SiC-C preforms used in this work were kindly provided by Petroceramic [47] as plates with dimensions of 25x25x5 mm. These preforms consist of a bimodal mixture of α-SiC particles (SiC_p), with particle sizes of 36.5 and 4.5 μm, incorporated into a C-matrix. SiC_p-C preforms were prepared by mechanically mixing α-SiC_p with phenolic resin (10wt%). The mixture was uniaxially pressed under a P = 140 MPa and at T = 150°C with resulting melt of the resin was melted and a strong cross-linking between α-SiC particles. The obtained green body was subsequently pyrolyzed under a N_2 atmosphere at T = 700ºC. During pyrolysis, the resin turned into C and a porosity was created inside the sample due to gas releasing of volatile products. Prior to the experiments, the SiC_p-C preforms (12x12x3 mm) were further thermally treated up to T = 1500°C to remove residual volatile compounds. In Table 1, the main characteristics of the SiC_p-C preform used in this work are detailed.

Tab. 1. Main characteristics of SiC_p-C Petroceramic preform.

The apparent density and He-density were accurately measured. As a result of three different measurements, apparent density in the range of 2.10-2.20 g/cm^3 and a He-density of 3.10 g/cm^3 were obtained, resulting in a porosity of 30.6%. Additionally, by Hg-porosimetry technique, the

pore size and the porous distribution were determined (see Table 1). In Table 1 the composition of each constituent is also reported. The composition was determined by thermo-gravimetric analysis (TGA) technique, under an inert atmosphere (N_2) in the range of T = 25-900ºC. The role of C is twice: as binder and as reactant/precursor in the production of additional SiC during reactive infiltration with liquid Si or Si-based alloys. In Figure 1, the microstructure and composition of the as received SiC_p-C preform, analyzed by SEM/EDS and X-ray diffraction, respectively are shown. By SEM analysis, two granulometries of SiC particles are well distinguished (light gray) as well as the C phase surrounding the SiC particles (black). As resulting by XRD analysis, α-SiC (as a mixture of the 4H and 6H polytypes) is the only crystalline phase detected in the preform.

Fig. 1. As received SiC_p-C preform: a) SEM image and b) XRD pattern.

The Si-62wt%Ir alloy samples (from now Si-Ir eutectic alloy), eutectic composition, were prepared by mixing high purity Ir and Si (99.98%-Goodfellow®). Eutectic alloy samples were produced with a weight of 50.0 mg for infiltration experiments. The alloy samples were produced by arc melting technique under an atmosphere of Ar (N60, O_2 < 0.1 ppm). Before the arc melting of Ir-Si alloys, the residual oxygen content inside the chamber was reduced by melting a Zr drop. To ensure the homogeneity of the alloy composition, the melting of every single Ir-Si sample was repeated 3 times. The as produced Ir-Si composition was checked on cross-sectioned sample both by SEM (to reveal eutectic microstructure) and XRD (to detect the phases) as shown in Figure 2.

Fig. 2. As-produced Si-62wt%Ir eutectic alloy by arc melting: a) SEM image at the cross-section and b) XRD pattern

2.2 Procedure and method

The goal of this experimental work is the study of the infiltration kinetics of both liquid Si and Si-Ir eutectic alloy into SiC_p-C porous preforms (see section 3). For infiltration experiments, an induction horizontal furnace was used and described in detail elsewhere [23,48].

Prior to the experiments, the metal sample was rinsed in ethanol + US and residual powder from the SiC_p-C preform was removed by compressed air.

At room temperature the Si/SiC_p-C and Si-Ir eutectic alloy/SiC_p-C couples were placed on a graphite plate/sample holder, introduced into the furnace and located at the central part of the heater. Once leveled the sample at horizontal plane, in order to remove any contaminant from the

experimental environment, the chamber was degassed under a vacuum (down to 10^{-4} Pa) for two hours.

The metal sample/substrate couple was heated under a vacuum by a 800 kHz high frequency generator coupled to a graphite susceptor ensuring an experimental surrounding atmosphere with reduced oxygen content ($PO_2 < 10^{-6}$ Pa). During all the experiments, the temperature was monitored by a pyrometer, previously calibrated by detecting the melting temperature of high purity metals (Sn, Al, Au, Cu, Si and Ni).

The infiltration experiments were performed by contact heating sessile drop method. The temperature was risen up to the testing temperature with a rate of 5°C/s. The selected temperature was kept constant until the complete infiltration of the preform, then the samples were "quenched" (cooling rate 10°C/s) to preserve the new formed interfaces and infiltrated microstructure. The evolution of infiltration experiments was monitored in real time and recorded (10 frames/sec) by a high resolution camera connected to a computer with an image analysis software ad hoc-developed (ASTRAVIEW®) [49]. The software allows the automatic acquisition of contact angles and drop geometric variables in real time (R-base radius and H-height). By analyzing such geometric variables as a function of time, is possible to follow the kinetics of infiltration with a great accuracy.

Owing to the different melting temperatures [46], (T = 1414°C for pure Si and T = 1222°C for Si-Ir eutectic alloy), different isothermal conditions for Si and Si-Ir eutectics infiltration experiments into SiC_p-C preforms were selected. Specifically, the testing temperature of T = 1450°C for Si/SiC_p-C and temperatures of T = 1250°C and T = 1350°C for the Si-Ir eutectic alloy/SiC_p-C, were imposed. At the end of the infiltration experiments, the samples were removed from the furnace, embedded into epoxy resin, cross-sectioned and metallographically mirror polished for microstructural characterization by SEM/EDS and XRD techniques.

3. Results and discussion

As already introduced, the present study aims to identify the mechanism mainly governing the infiltration of SiC_p-C preforms: either driven by chemical reaction or by fluido-dynamics. Firstly, it is important to note that infiltration of SiC_p-C preforms with both metal materials, pure Si and Si-Ir eutectic alloy, took place spontaneously and complete infiltration of SiC_p-C preforms was rapidly achieved. On the other hand, since the C content in this preform is quite low (4.7wt%), porosity and pore diameter should not substantially change during infiltration.

In order to define the main driving force governing infiltration, a careful analysis of infiltration kinetics is necessary to be performed. As reported by [52], the infiltration kinetics can be

analyzed by following the evolution of the height of infiltration (*h inf*) (i.e. infiltration depth), usually described by linear, parabolic or other laws [53,54]. It is possible to calculate *h inf* by assuming that a spherical cap geometry of the molten drop is preserved during infiltration process. This basic assumption enables to analyze the infiltration kinetics by simply following the behaviors of contact angles and drop geometrical parameters such as the drop base radius (*R*) and the h-drop height (*h*) as a function of time (see Figure 4). By using the following equation 2, it is easy to calculate the emerging drop volume (*V*) as a function of time.

$$V = \frac{\pi h}{6}(3{R_B}^2 + h^2) \quad (2)$$

By knowing the initial volume of the drop (V_0), the infiltrated volume (V_{Inf}), can be calculated as:

$$V_{Inf} = V_0 - V \quad (3)$$

Similar infiltration studies on C/Al-Si [55] and C/Ni-Si [56] systems are reported in literature, where the abovementioned description and interpretation of the results was applied.

In particular, this model describes the infiltrated volume accordingly to a shape of a truncated cone (as shown in Figure 3), where the bottom diameter takes a flat shape, which corresponds to the drop base diameter at the beginning of the infiltration process ($D_0 = 2R_0$). In addition, the upper diameter of the infiltrated area is equal to the final base diameter ($D_f = 2R_f$).

Fig. 3. Schematic drawing of the drop with the infiltrated area at the beginning and at the end of the infiltration process [55, 56].

According to equations describing a truncated cone and knowing material porosity (α_{ef}), the infiltration height (h_{Inf}) can be calculated as a function of time as follows:

$$h_{Inf}(t) = \frac{1}{\alpha_{ef}}\left(\frac{3\,V_{Inf}}{\pi\,(R^2 + {R_0}^2 + RR_0)}\right) \quad (4)$$

As mentioned above, the infiltration experiments were performed on SiC_p-C preforms, by infiltrating pure Si at T = 1450°C and Si-Ir eutectic alloys at T = 1250°C and T = 1350°C, as shown in Figure 4. The evolution of advancing contact angle and drop geometric parameters (H-drop height and R-drop base radius) are reported from the drop melting until its complete infiltration into SiC_p-C porous preforms.

Fig. 4. Evolution of contact angles and drop geometric variables (R-drop base radius and H-drop height) recorded within the infiltration experiments performed on SiC_p-C/Si at T = 1450°C and SiC_p-C/Si-Ir eutectic alloy at T = 1250°C, 1350°C; a) evolution of contact angle, b) evolution of normalized drop height and c) evolution of normalized base radius, d) stages in the evolution of the normalized base radius.

At first glance, the infiltration of SiC_p-C by pure Si (at T ≈ Tm + 30°C) occurred faster (one order of magnitude) than Si-Ir eutectics at T = 1250°C (≈ 30°C above the melting point). As expected, the temperature strongly influenced the infiltration process is strongly temperature-dependent, since the increase of 100°C in the testing temperature (at T = 1350°C, see Figure 4a and 4b) substantially increases of ~ 7 times the infiltration time required for the complete infiltration: t = 25 sec at T = 1350°C and t = 170 sec at T = 1250°C. In addition, 2 stages are well distinguished in the infiltration kinetics (see Figure 4d). Within the first (I stage), the drop radius increased up to a maximum value due to capillary forces and consequently an enlargement of the infiltration front in terms of R ($R_0 < R < R_{fl}$) was observed where $R_{MAX} = R_{fl}$. At the maximum value of drop radius, a second phenomenon is observed (II stage), where the radius decreased progressively due to the appearance of hydrodynamic action [57]. Interactions between the molten drop and the porous substrate strongly influence the kinetics of each stage. Several studies performed on metal infiltration into porous substrates [58,59] already reported about the presence of two competitive processes observed during the first stage: drop spreading process and infiltration process, as shown in Figure 5.

Fig. 5. Scheme of competition between spreading and infiltration and related shape of the drop during infiltration process. U_{spr} = spreading rate and U_{inf} = infiltration rate.

In Figure 6, as further evidence, the time sequence for the mentioned infiltration experiments, by collecting the more significant recorded images, is shown. It is important to note that molten drops preserved a regular spherical cap shape through all the infiltration process. Moreover, the kinetics of spreading clearly varied upon the infiltrating material and temperature. In the case of the Si-infiltration, absence of drop spreading was observed ($U_{spr} << U_{inf}$ case b, as shown in Figure 5).

On the contrary, analyzing the alloy behavior, the competition between spreading and infiltration is more pronounced ($U_{spr} \approx U_{inf}$ case c, as shown in Figure 5) since the maximum radius is higher than the initial equatorial radius.

Fig. 6. Images of drop profiles recorded during infiltration experiments performed on SiC_p-C preforms with: a) Si at T = 1450°C, b) Si-Ir eutectic alloy at T = 1350°C and c) Si-Ir eutectic alloy at T = 1250°C.

In order to well interpret the different behaviors observed, a study of infiltration kinetics was carried out using the model presented in equation 4. Figure 7 shows the evolution of emerging drop volume (V), infiltrated volume (V_{inf}) and height of infiltration (h_{inf}) as a function of the experimental conditions. As it can be seen, infiltration kinetics ($h_{inf}\ (t)$) are well described by linear equation, thus deviating from the Darcy's parabolic law [60, 61]. In the experiment carried out with pure Si at T = 1450°C, a weak deviation from linearity was observed within the first 3 seconds, cause the drop movements during the melting (see time sequence reported in Figures 6a and 7a) and delay in taking its spherical shape, mainly due to the presence of a layer of native SiO_2 oxide. The agreement between infiltration kinetics and linear law description of the phenomenon, is typical of interactions process mainly dominated by chemical reaction [60-62].

Fig. 7. Evolution of drop emerging volume (V), infiltrated volume (V_{inf}), and height of infiltration (h_{inf}) for experiments performed on SiC_p-C porous preforms by infiltrating: a) and b) pure Si at T = 1450°C; c) and d) Si-Ir eutectic alloy at T = 1250°C and e) and f) Si-Ir eutectic alloy at T = 1350°C. The linear equation and standard deviation are inserted.

Different equilibria/chemical reactions occuring within the infitration process, at early-stage at the surface and following at the pore walls, drive the continuous advancing of infiltration of the metal phase into the SiC_p-C preform [63]. In particular, during the interaction between the Si melt phase and the preform, the reaction between C and Si took place producing as reaction products SiC and Ir-silicide ($IrSi_3$). In addition, in contact with melt Si phase, the primary SiC underwent to dissolution and re-precipitation (secondary SiC) as documented by [64]. Moreover, it is worth to be mentioned that Si and Si-based alloys well wet SiC [65]. Finally, the reaction kinetics is increased in the case of pure Si, being C-solubility in liquid Si very low and saturation quickly achieved [66].

In Figure 8, SEM images of the cross-sectioned Si-infiltrated sample at T = 1450° C are shown.

Fig. 8. BSE images of the microstructure after the infiltration of SiC_p-C preforms by pure Si at T = 1450°C: a) global infiltration area and b), c) and d) details of the resulting microstructure at higher magnifications in particular of infiltrated area 1 and 2.

Analyzing the infiltration front in Figure 8, two different infiltrated microstructures can be observed (area 1 and area 2, see Figure 8b). In particular, in the area 1 (Figure 8c), unreacted Si is still present (bright phase) surrounding the SiC particles. In parallel, as shown in Figure 8d, absence of unreacted Si is detected at the border of the infiltration front. However, a higher degree of SiC_p-consolidation by newly produced SiC is evident, might be given by reaction between C and evaporated/condensated Si from the area 1. This evidence, together with the

linear behavior of infiltration height as a function of time, let us to state that the reactivity is the main phenomenon driving infiltration process. The same conclusion might be predicted when the infiltrating material is Si-Ir eutectics. The final microstructure of SiC_p-C infiltrated with liquid Si-Ir eutectic alloy at T = 1250°C is shown in Figure 9. Owing to comparable size, it is not possible to distinguish between pre-existing SiC particles and new produced and growth SiC crystals by the reaction between Si and C during infiltration process [23]. A further evidence that infiltration was driven by reaction even for Si-Ir eutectic alloy, is the resulting activation energy. To calculate activation energy, some kinetic parameters need to be preliminarily determined, such as the infiltration rate (U_{inf}). In Table 2 the values of infiltration rate (U_{inf}), spreading rate (U_{spred}) and their ratio itself, as a function of temperature and the metal material used, are reported.

Fig. 9. BSE images of SiC_p-C preform microstructure infiltrated with liquid Si-Ir eutectic alloy at T = 1250°C. a) global microstructure of infiltrated area and b) detail of the infiltration front at higher magnification.

Tab. 2. Kinetic parameters (U_{inf}-infiltration and U_{spred}-spreading rates) calculated for infiltration experiments of SiC-C preforms with pure Si and Si-62wt.% Ir alloy, carried out at T = 1450°C, T = 1250°C and T = 1350°C, respectively.

Since the infiltration kinetics is linear with the time, the infiltration rate U_{inf} (= dh_{inf} /dt) is constant and equal to the slope of h_{inf} *(t)*. The spreading rate U_{esp} (= dR/dt), was calculated by the slope of the quasi-linear area of the curve R(t). Two aspects are deserving to be highlighted: as a first, the infiltration rate is greater of one order of magnitude than the value reported for graphite infiltrated with Ni-Si system [52] even though the permeability is lower. Another important aspect deserving attention, although the tortuosity is greater than the value reported in [52], in all cases the infiltration rate is comparable or even higher than the spreading one. By using Arrhenius equation and calculating infiltration rate of Si-Ir eutectic alloy into SiC_p-C preform for two different temperatures, a value of the activation energy Ea_{inf} = 330 kJ/mol is resulting. The calculated Ea is in a good agreement with values reported around few hundred kJ/mol on reactive infiltration processes previously studied [46]. This range of Ea values discriminates between infiltration process driven by chemical reaction respect to infiltration driven by viscous resistance where the activation energy is usually resulting around tens of kJ/mol [67].

3.2 Microstructural characterization of the as produced composites

As aforementioned in the previous sections, SiC/Si and SiC/$IrSi_3$ composites were produced by Si and Si-62wt.% Ir eutectics infiltration into SiC_p-C preforms at T = 1450°C and T = 1350°C,

respectively. In both cases metal infiltration took place spontaneously and complete infiltration of preforms were achieved within a dwell time of less than 5 min. At the end of the infiltration process, samples were removed from the furnace and abraded to remove the exceeding metal material.

As a first, the density of the as produced composites was measured: 2.80 ± 0.05 g/cm^3 for SiC/Si and 6.35 ± 0.19 g/cm^3 for SiC/$IrSi_3$, resulting in residual porosity of 4.9% and 6.4%, respectively.

SEM analyses on the cross-sectioned composite materials were performed. The microstructures of the as produced SiC/Si and SiC/$IrSi_3$ composites are shown in Figure 10 at different magnifications. At lower magnification, a high-dense microstructure with limited porosity is the first evidence: the pre-existing pores were completely filled by metal material. Furthermore, no evidence of cracks or interface detachments between the matrix and reinforcement were detected, demonstrating excellent thermal compatibility between the phases.

Focusing on SiC/Si composite, by SEM/EDX (see Figures 10a and 10b), and X-ray diffraction (see Figure 11a), SiC (dark grey) and Si (bright) phases were detected. In addition, absence of unreacted C was either detected.

Fig. 10. SEM analyses (retro-scattered electrons) of cross-sectioned composite materials: a) and b) SiC/Si produced at T = 1450°C; and c) and d) SiC/$IrSi_3$ produced at T = 1350°C.

Regarding SiC/$IrSi_3$ composites, three different phases were detected by XRD (Figure 11b): SiC, Si and $IrSi_3$. SiC particles with three different sizes: 36.5, 4.5 and 1-2 μm (see Figures 10c and 10d). The SiC particles with lower size were produced during infiltration process (secondary SiC) by reaction of Si with C. In the area surrounding the SiC particles, a Si-$IrSi_3$ eutectic phase is detected. Finally, as for SiC/Si, a residual porosity is still present into SiC/$IrSi_3$ produced composite.

As a general conclusion, both produced composites show a highly-dense isotropic (homogeneous) microstructure, key features to obtain high thermo-mechanical response.

Fig. 11. X-ray diffraction patterns of composite materials: a) SiC/Si produced at T = 1450°C and b) SiC/$IrSi_3$ produced at T = 1350°C

4. Conclusions

For the first time, the feasibility to infiltrate SiC_p-C porous preforms (bimodal SiC particles bonded by C) by pure Si and Si-62wt%Ir eutectic alloy was successfully tested. For both the metal phases, the infiltrations of SiC_p-C preforms took place spontaneously and highly-dense, nearly-shaped SiC/Si and SiC/$IrSi_3$ composites were effortless produced. The presence of free C as bonding phase played a key role in driving the reactivity and kinetics within infiltration experiments. Since C is on the pore wall (bonding the bimodal SiC-particles) both infiltrations processes were mainly governed by SiC formation at the infiltration front.

Taking into account that:

1) the infiltration kinetics is well described by linear law;

2) the resulting activation energy is 330 KJ/mol;

3) highly consolidated SiC particles is observed by the appearance of secondary SiC;

let us to conclude that the infiltration process is mainly driven by reactivity.

However, the higher infiltration rate measured respect to similar experiments performed by infiltrating Si and Si-based alloys into porous graphite, together with the irregular infiltration fronts observed, suggests that capillarity and viscous forces might play a concomitantly role.

To better understand the overall infiltration process, a parallel investigation on the interactions at Si-Ir alloys/C-based materials interfaces by studying the wettability and spreading kinetics as a function of operating conditions is ongoing.

Acknowledgements

The work performed at the University of Alicante was funded by the Spanish "Ministerio de Economía y Competitividad" (Grant MAT2017-86992-R), and action Mobility of Alicante University. The work performed at CNR-ICMATE was supported by National Science Center of Poland through POLONEZ project number UMO-2016/23/P/ST8/01916. This project is carried out under POLONEZ-3 program which has received funding from European Union's Horizon 2020 research and innovation program under Marie Skłodowska-Curie grant agreement. No 665778.

DG wishes to thank Dr Vincenzo Buscaglia for the critical reading and his suggestions made to improve the manuscript. The authors would like to acknowledge Dr Maurizio Valle (Petroceramics s.r.l) for kindly providing the SiC_p preforms used in this investigation.

References

[1] D.D.Chung, Composite Materials Science and Applications, Springer-Verlag London, 2010.

[2] I.M. Low, Ceramic Matrix Composites: Microstructure, Properties and Applications, Woodhead Publishing, 2006.

[3] R. Novakovic, B. Korthaus, Advanced Ceramics for Use in Highly Oxidizing and Corrosive Environments: Siliconised Silicon Carbide. Key Eng. Mater. 201 (2001) 141–182. https://doi.org/10.4028/www.scientific.net/KEM.201.141

[4] F. Cardarelli, Materials Handbook A Concise Desktop Reference, Springer-Verlag London, 2018.

[5] M. Srinivasan, Structural Ceramics, Academic Press, London, 1989.

[6] S. Prochazka, R.M. Scanlan, Effect of Boron and Carbon on sintering of SiC, J. Am. Ceram. Soc. 58 (1975) 72.

[7] F. Lange, T.K. Gupta, Sintering of SiC with boron compounds, J. Am. Ceram. Soc. 59 (1976) 537–538.

[8] J. Lis, Y. Miyamoto, R. Pampuch, K. Tanihata, Ti_3SiC-based materials prepared by HIP-SHS techniques, Mater. Lett. 22 (1995) 163–168. https://doi.org/10.1016/0167-577X(94)00246-0.

[9] E. Gomez, J. Echeberria, I. Iturriza, F. Castro, Liquid phase sintering of SiC with additions of Y_2O_3, Al_2O_3 and SiO_2, J. Eur. Ceram. Soc. 24 (2004) 2895–2903. https://doi.org/10.1016/j.jeurceramsoc.2003.09.002

[10] N. R. Calderon, M. Martinez-escandell, J. Narciso, F. Rodriguez-reinoso, Manufacture of biomorphic SiC components with homogeneous properties from sawdust by reactive infiltration with liquid silicon, J. Amer. Ceram. Soc. 93 (2010) 1003–1009. https://doi.org/10.1111/j.1551-2916.2009.03572.x

[11] N. R. Calderon, M. Martinez-escandell, J. Narciso, F. Rodriguez-reinoso, The combined effect of porosity and reactivity of the carbon preforms on the properties of SiC produced by reactive infiltration with liquid Si, Carbon 47 (2009) 2200–2210. https://doi.org/10.1016/j.carbon.2009.04.002

[12] Y. Tong, S. Bai, X. Liang, Q. H. Qin, J. Zhai, Reactive melt infiltration fabrication of C/C-SiC composite: wetting and infiltration, Ceram. Int. 42 (15) (2016) 17174–17178. https://doi.org/10.1016/j.ceramint.2016.08.007.

[13] Y. Xie, L. Cheng, L. Li, H. Mei, L. Zhang, Strengthening/toughening of laminated SiC_w/SiC ceramic composites by heat treatment, Ceram. Int. 41 (2015) 10024–10029. https://doi.org/10.1016/j.ceramint.2015.04.087

[14] D. Kopeliovich, Advances in the manufacture of ceramic matrix composites using infiltration techniques. Advances in Ceramic Matrix Composites, 2014.

[15] S.T. Mileiko, Carbon/Carbon, Cement, and Ceramic Matrix Composites, Comprehensive Composite Materials, 2000.

[16] J.N. Ness, T.F. Page, Microstructural evolution in reaction-bonded silicon carbide, J. Mater. Sci. 21 (1986) 1377–1397.

[17] A.J. Whitehead, T.F. Page, Fabrication and characterization of some novel reaction-bonded silicon carbide materials, J. Mater. Sci. 27 (1992) 839–852.

[18] M. Caccia, J. Narciso, SiC manufacture via reactive infiltration, Processing and Properties of Advanced Ceramics and Composites VI: Ceramic Transactions, John Wiley & Sons, 2014.

[19] M. Caccia, J. Narciso, Production of SiC Materials by Reactive Infiltration, Mater. Sci. Forum 783–786 (2014) 1863–1866. https://doi.org/10.4028/www.scientific.net/MSF.783-786.1863

[20] J.F. Narciso-Romero, R. Arpón-Carballo, Synthesis of mixed disilicides/SiC composites by displacement reaction between metal carbides and silicon, J. Ceram. Soc. Jpn. 108 (2000) 957–959. https://doi.org/10.1016/j.msea.2004.03.052

[21] D. Y. Oh, H. C. Kim, J. K. Yoon, I. Ko, I. J. Shon, One step synthesis of dense $MoSi_2$-SiC composite by high-frequency induction heated combustion and its mechanical properties, J. Alloy Comp. 395 (1-2) (2005) 174–180. https://doi.org/10.1016/j.jallcom.2004.10.072

[22] M. Caccia, C. Xiang, J. Narciso, N. Gupta, Reactive melt infiltration as synthesis route for enhanced SiC/$CoSi_2$ composite materials for advanced armor systems, Ceram. Int. 44 (11) (2018) 13182-13190. https://doi.org/10.1016/j.ceramint.2018.04.143

[23] M. Caccia, S. Amore, D. Giuranno, E. Ricci, J. Narciso, Towards optimization of SiC/$CoSi_2$ composite material manufacture via reactive infiltration: Wetting study of Si–Co alloys on carbon materials, J. Eur. Ceram. Soc. 35 (15) (2015) 4099-4106. https://doi.org/10.1016/j.jeurceramsoc.2015.07.016

[24] O. C. Esteban, M. Caccia, A. Camarano, J. Narciso, Advances in High Temperature Ceramic Matrix Composites and Materials for Sustainable Development; Ceramic Transactions, John Wiley & Sons, 2017.

[25] P. J. Meschter, D. S. Schwartz, Silicide-matrix materials for high-temperature applications, J. Miner. Met. Mater. Soc. 41(1989) 52–55. https://doi.org/10.1007/BF03220384

[26] B. E. K. Ohriner, Processing of iridium and iridium alloys, Platin. Met. Rev. 52 (2008)186–197. doi:10.1595/147106708x333827.

[27] I. Iavicoli, V. Leso, Iridium. Handbook on the Toxicology of Metals (eds. G. Nordberg, B. Fowler, M. Nordberg, Academic Press, 2014). https://doi.org/10.1016/C2011-0-07884-5

[28] R. Crabtree, Iridium compounds in catalysis, Acc. Chem. Res. 12 (9) (1979) 331–337. doi: 10.1021/ar50141a005

[29] S. B. Singh, Green Chemistry & Technology Letters 2 (4) (2016) 206-210. doi: 10.18510/gctl.2016.247

[30] W.D. Huang, H. Cao, S. Deb, M. Chiao, J.C. Chiao, Iridium oxide based coaxial pH ultramicroelectrode, Sensors and Actuators A 169 (2011) 1-11. https://doi.org/10.1016/j.elecom.2013.12.012

[31] S. Vasudevan, Anodes for Electrochemcial Processes (Part-I), Res. J. Chem. Sci 3 (5) (2013) 1-2.

[32] D. R. Lide, CRC Handbook of Chemistry and Physics. (CRC Press, 2010).

[33] Y. Y. Mitarai, Y. Ro, T. Maruko, H. Harada, Ir-base refractory superalloys for ultra-high temperatures, Met. Mat. Trans. A 29 (1998) 537-549. https://doi.org/10.1007/s11661-998-0135-9

[34] K. Mumtaz, J. Echigoya, M. Taya, Thermal cycling of iridium coatings on isotropic graphite, J. Mater. Sci. 28 (1993) 5521–5527. https://doi.org/10.1007/BF00354413

[35] J. R. Strife, J. G. Smeggil, W. L. Worrell, Reaction of Iridium with Metal Carbides in the Temperature Range of 1923 to 2400 K, J. Am. Ceram. Soc. 73 (1990) 838–845. https://doi.org/10.1111/j.1151-2916.1990.tb05123.x

[36] National Research Council. High-Temperature Oxidation-Resistant Coatings: Coatings for Protection From Oxidation of Superalloys, Refractory Metals, and Graphite. (The National Academies Press, 1970).

[37] Y. Huang, S. Bai, H. Zhang, Y. Ye, L. Zhu, Oxidation of Iridium coatings on rhenium substrates at ultrahigh temperature in stagnant air: its failure mechanism and life model, Surf. Coatings Technol. 288, (2016) 52–61. https://doi.org/10.1016/j.surfcoat.2016.01.004

[38] Z. Chen, Iridium Coating: Processes, Properties and Application. Part I. Johnson Matthey Technol. Rev. 61 (2017) 16–28. http://dx.doi.org/10.1595/205651317X693606

[39] J. C. Hamilton, Diffusion mechanisms in chemical vapor-deposited iridium coated on chemical vapor-deposited rhenium, Metall. Trans. A 23 (1992) 851–855. https://doi.org/10.1007/BF02675562
[40] J. B. Sha, & Y. Y. Mitarai, Ir–Nb–Si ternary refractory superalloys with a three-phase fcc/$L1_2$/silicide structure for high-temperature applications, Intermetallics 14 (2006) 672–684. https://doi.org/10.1016/j.intermet.2007.07.001
[41] K. L. Luthra, US Patent - N 5,080,862 - Iridium Silicon alloy. (1992).
[42] S. T. Prisbrey, US Patent, N 6,759,141 - Oxidation preventative capping layer for deep-ultra-violet and soft x-ray multilayers. 1 (2004).
[43] C. A. Swenson, Recommended Values for the Thermal Expansivity of Silicon from 0 to 1000 K, J. Phys. Chem. Ref. Data 12 (1983) 179–182. https://doi.org/10.1063/1.555681
[44] J. J. Halvorson, R. T. Wimber, Thermal Expansion of Iridium at High Temperatures, J. Appl. Phys. 43 (1972) 2519–2522. https://doi.org/10.1063/1.1661553
[45] Z. Li, R. C. Bradt, Thermal expansion of the cubic (3C) polytype of SiC, J. Mater. Sci. 21 (1986) 4366–4368. doi: 10.1007/BF01106557
[46] H. Okamoto, Ir-Si (Iridium-Silicon). J. Phase Equilibria Diffus. 28 (2007) 495. doi: 10.1007/s11669-007-9151-5
[47] Petroceramic. Available at: http://www.petroceramics.com/
[48] D. Giuranno, S. Delsante, G. Borzone, R. Novakovic, Effects of Sb addition on the properties of Sn-Ag-Cu/(Cu, Ni) solder systems, J. Alloys and Compounds, 689 (2016) 918-930. https://doi.org/10.1016/j.jallcom.2016.08.035
[49] L. Liggieri, A. Passerone, An automatic technique for measuring the surface tension of liquid metals, High Temp. Technol. 7 (1989) 82–86. https://doi.org/10.1080/02619180.1989.11753417
[50] G. R. Anstis, P. Chantikul, B.R. Lawn, D.B. Marshall, A Critical Evaluation of Indentation Techniques for Measuring Fracture Toughness: I, Direct Crack Measurements, J. Am. Ceram. Soc. 64 (1981) 533–538. https://doi.org/10.1111/j.1151-2916.1981.tb10320.x
[51] G. D. Quinn, R. C. Bradt, On the Vickers Indentation Fracture Toughness Test, J. Am. Ceram. Soc. 90 (2007) 673–680. https://doi.org/10.1111/j.1551-2916.2006.01482.x
[52] R. Voytovych, V. Bougiouri, N. R. Calderon, J. Narciso, N. Eustathopoulos, Reactive infiltration of porous graphite by NiSi alloys, Acta Mater. 56 (2008)2237–2246. https://doi.org/10.1016/j.actamat.2008.01.011
[53] E. Louis, J.A. Miralles, J.M. Molina, High temperature infiltration at low overpressures: Darcy's law, the slug-flow hypothesis and percolation, J Mater Sci 50 (2015) 1655–1665. doi: 10.1007/s10853-014-8726-x
[54] E. Louis, J.A. Miralles, J.M. Molina, Reactive infiltration: identifying the role of chemical reactions, capillarity, viscosity and gravity, J Mater Sci 52 (2017) 7530–7538. doi10.1007/s10853-017-0985-x
[55] N. R. Calderon, R. Voytovych, J. Narciso, N. Eustathopoulos, Pressureless infiltration versus wetting in AlSi/graphite system, J. Mater. Sci. 45 (2010) 4345–4350. Doi: 10.1007/s10853-010-4358-y
[56] V. Bougiouri, R. Voytovych, N.Rojo-Calderon, J.Narciso, N. Eustathopoulos, The role of the chemical reaction in the infiltration of porous carbon by NiSi alloys, Scr. Mater. 54 (2006) 1875–1878. https://doi.org/10.1016/j.scriptamat.2006.02.015
[57] V. M. Starov, S. A.Zhdanov, S. R. Kosvintsev, V. D. Sobolev, M. G.Velarde, Adv. Colloid Interface Sci. 104 (2003) 123–158.
[58] A. Clarke, T. D. Blake, K. Carruthers, A.Woodward, Spreading and Imbibition of Liquid Droplets on Porous Surface, Langmuir 18 (2002) 2980–2984.
[59] H. R. Charles-Williams, R. Wengeler, K. Flore, H. Feise, M.J. Hounslow, A.D. Salman, Granule nucleation and growth: Competing drop spreading and infiltration processes,

Powder Technol. 206 (2011) 63–71. https://doi.org/10.1016/j.powtec.2010.06.013
[60] C. Garcia-Cordovilla, E. Louis, J. Narciso, Pressure infiltration of packed ceramic particulates by liquid metals, Acta Mater. 47 (1999) 4461–4479. https://doi.org/10.1016/S1359-6454(99)00318-3
[61] M. Caccia, A. Camarano, D. Sergi, A. Ortona, J. Narciso, Wetting and Navier-Stokes Equation — TheManufacture of Composite Materials, Wetting and Wettability (ed. by M. Aliofkhazraei, Intech, 105-138, 2015).
[62] N. Eustathopoulos, Wetting by Liquid Metals — Application in Materials Processing: The Contribution of the Grenoble Group, Metals, 5 (2015) 350–370. doi:10.3390/met5010350
[63] O. Dezellus, S. Jacques, F. Hodaj, N. Eustathopoulos, Wetting and infiltration of carbon by liquid silicon, J. Mater. Sci. 40 (2005) 2307–2311. https://doi.org/10.1007/s10853-005-1950-7
[64] Drevet, N. Eustathopoulos, Wetting of ceramics by molten silicon and silicon alloys: a review, J. Mater. Sci. 47 (2012) 8247–8260. doi: 10.1007/s10853-012-6663-0
[65] G.W. Liu, M.L. Muolo, F. Valenza, A. Passerone, Survey on wetting of SiC by molten metals, Ceram. Int. 36 (2010) 1177–1188. https://doi.org/10.1016/j.ceramint.2010.01.001
[66] L. Jian-Guo, H. Hans, Reactive Wetting in the Liqui-Silicon/Solid-Carbon System, J. Am. Ceram. Soc. 79 (1996) 873–880. https://doi.org/10.1111/j.1151-2916.1996.tb08519.x
[67] R. Israel, R. Voytovych, P. Protsenko, B. Drevet, D. Camel, N. Eustathopoulos, Capillary interactions between molten silicon and porous graphite, J. Mater. Sci. 45 (2010) 2210–2217. doi: 10.1007/s10853-009-3889-6

Table

Property		**Value**	**Unit**
Density	Apparent density	2,10-2,20	g/cm^3
	Helium density	3,10	g/cm^3
Porosity	Porosity (α_{ef})	30,6	%
	Medium pore diameter	1,3	µm
Composition	Silicon carbide (α-SiC)	95,3	wt.%
	Carbon binder (C)	4,7	wt.%

Tab. 1. Main characteristics of SiC_p-C Petroceramic preform.

Table

Metal	T (°C)	U_{inf} (µm/s)	U_{esp} (µm/s)	U_{inf} / U_{esp}
Si	1450	375,0	33,4	11,2
Si-62wt.%Ir	1250	12,1	7,0	1,73
Si-62wt.%Ir	1350	60,1	49,2	1,22

Tab. 2. Kinetic parameters (U_{inf}-infiltration and U_{spred}-spreading rates) calculated for infiltration experiments of SiC-C preforms with pure Si and Si-62wt.% Ir alloy, carried out at T = 1450°C, T = 1250°C and 1350°C, respectively.

Figure
Click here to download high resolution image

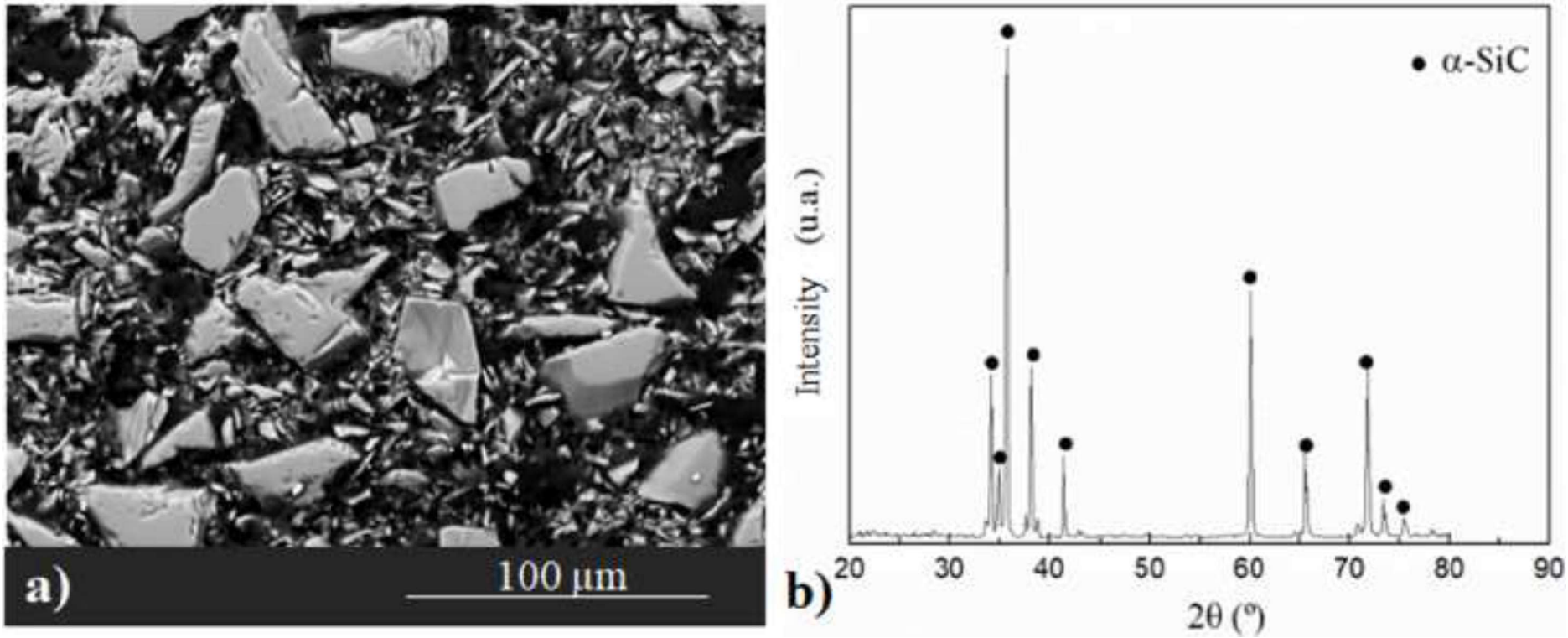

Figure
Click here to download high resolution image

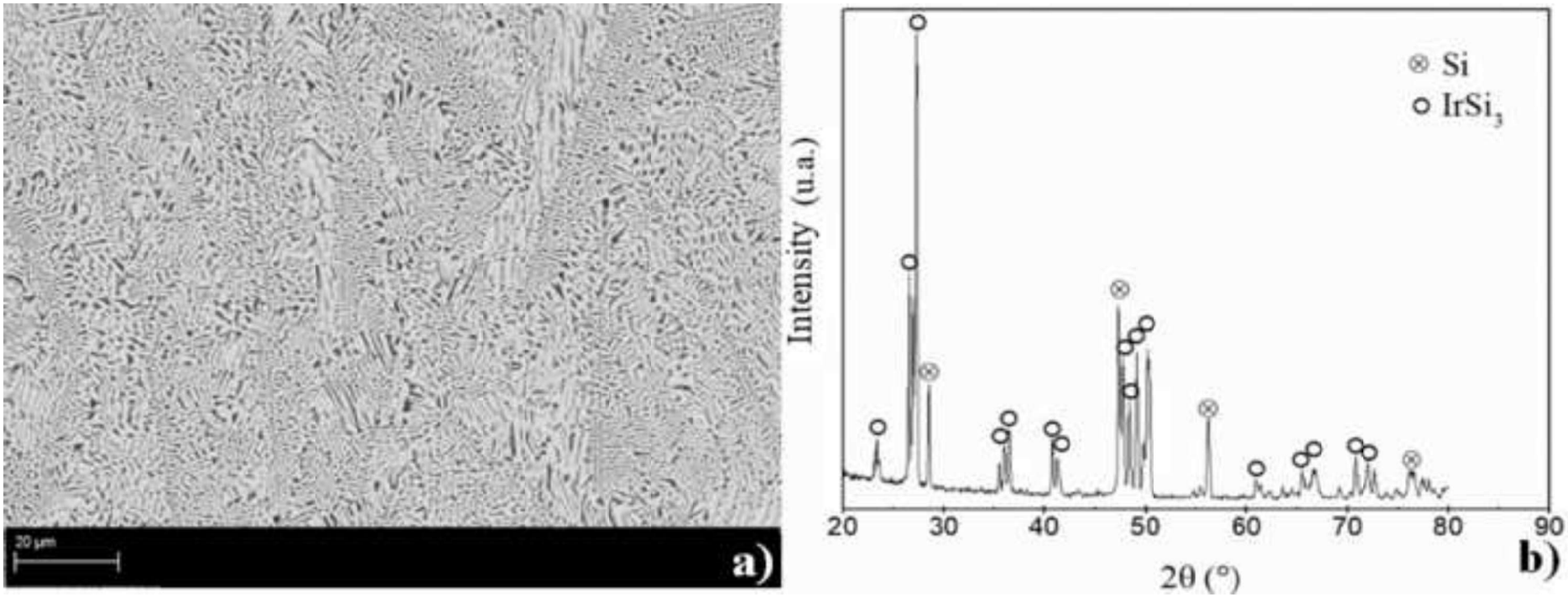

Figure
Click here to download high resolution image

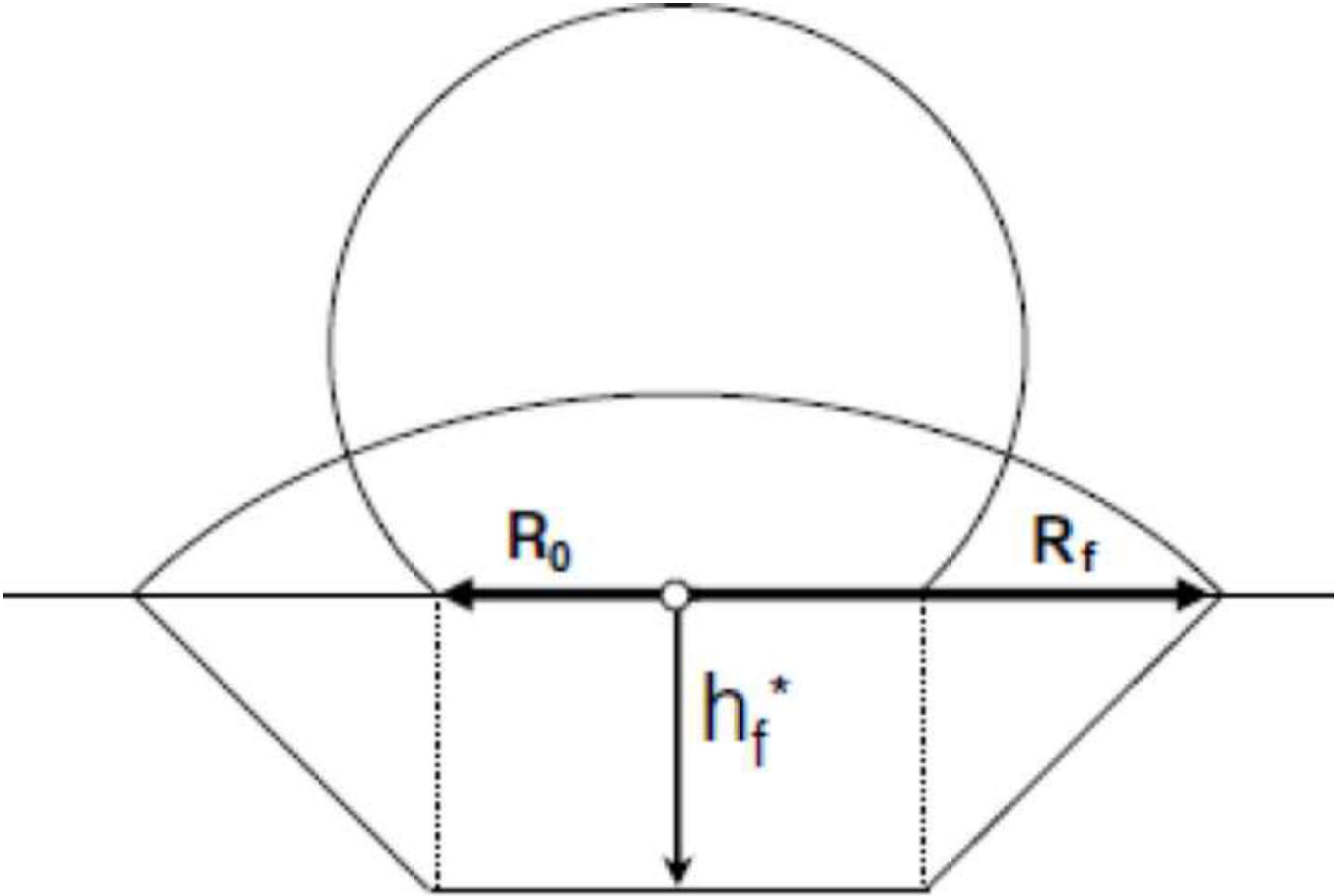

Figure

Click here to download high resolution image

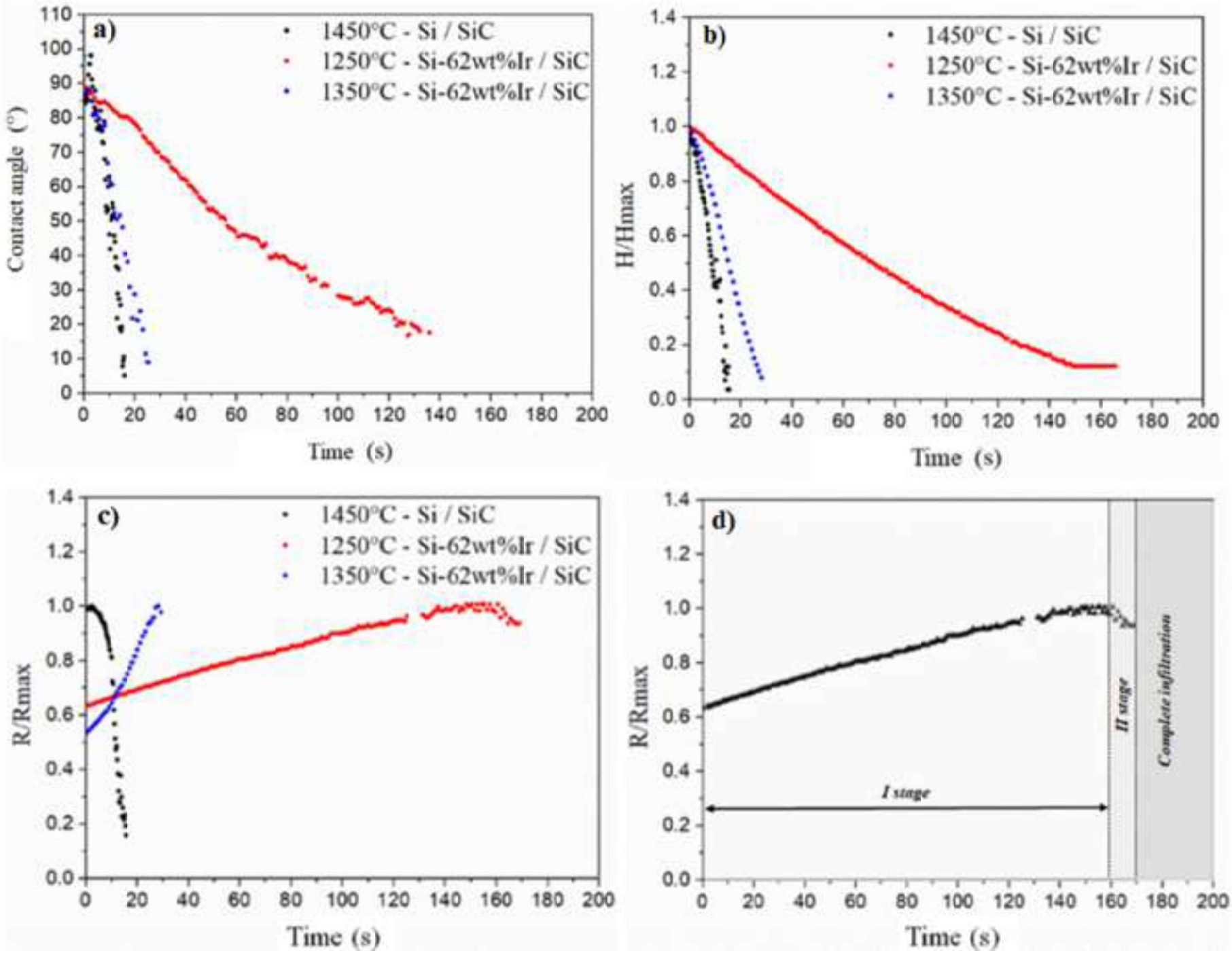

Figure
Click here to download high resolution image

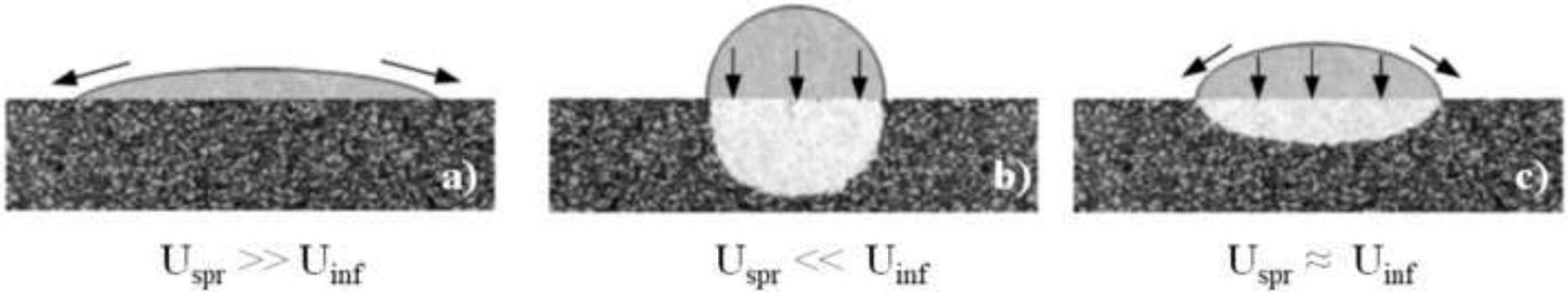

Figure
Click here to download high resolution image

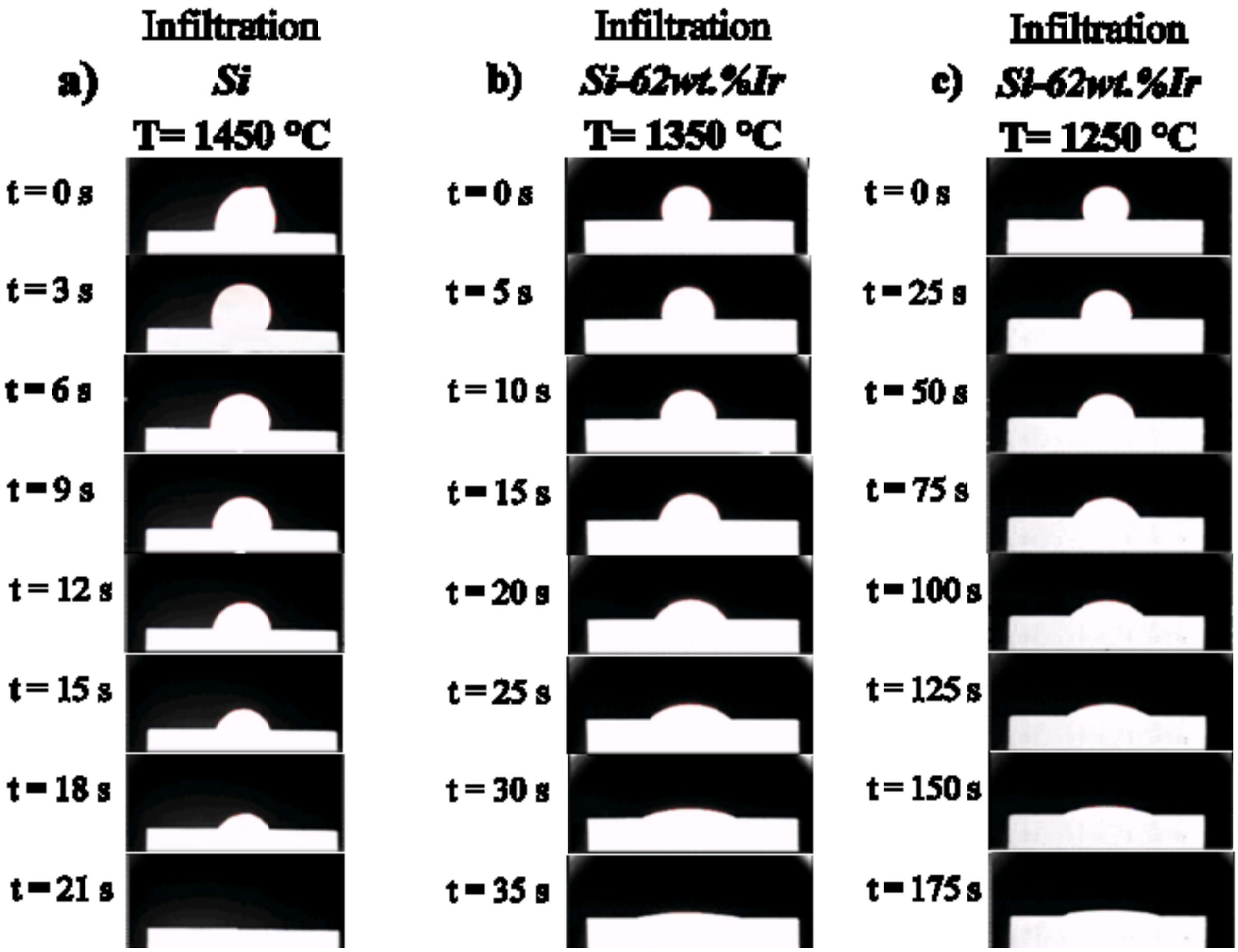

Figure
Click here to download high resolution image

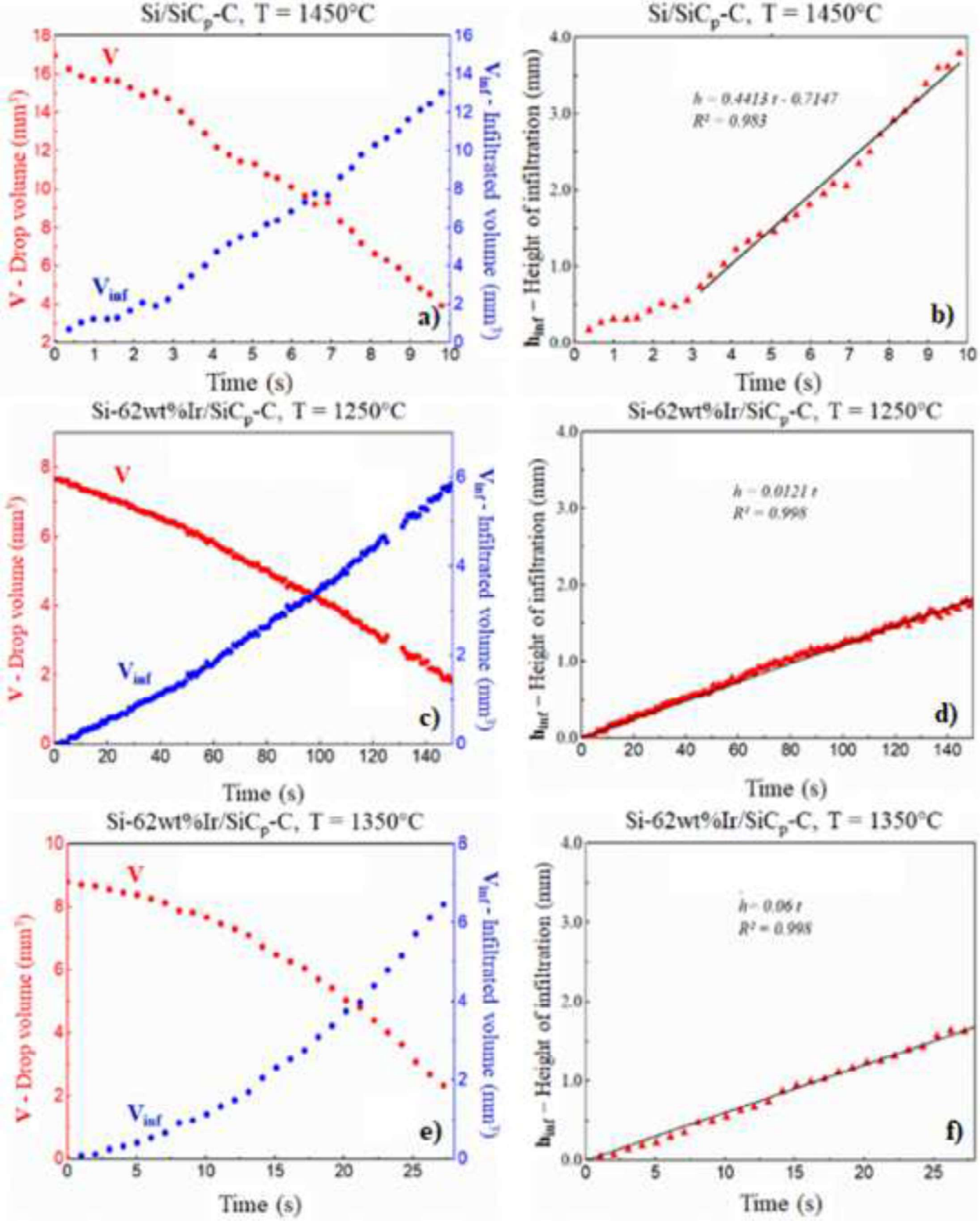

Figure
Click here to download high resolution image

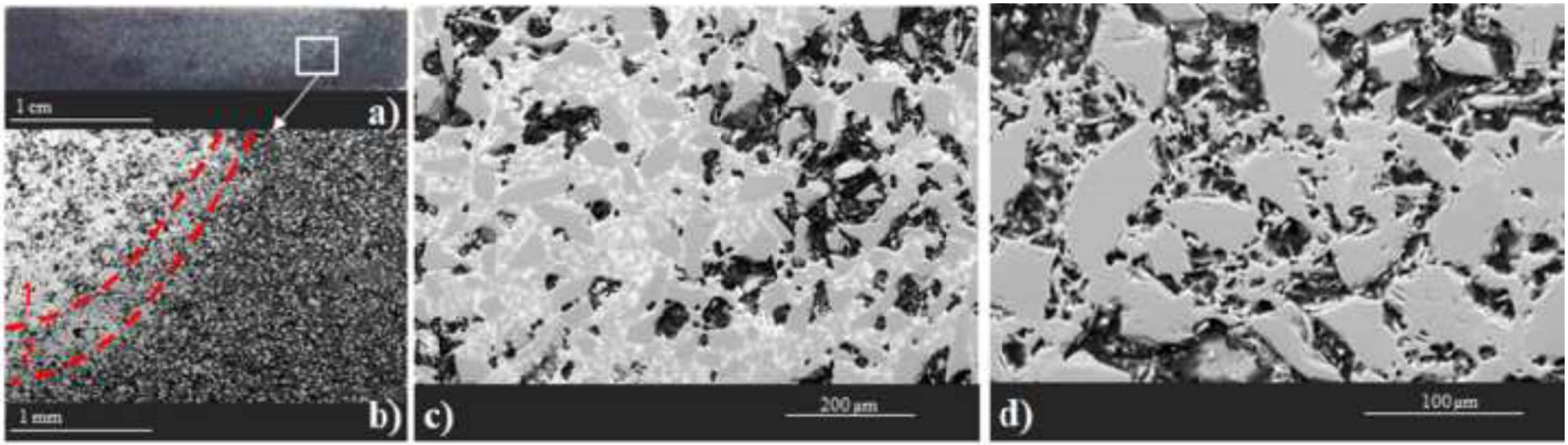

Figure
Click here to download high resolution image

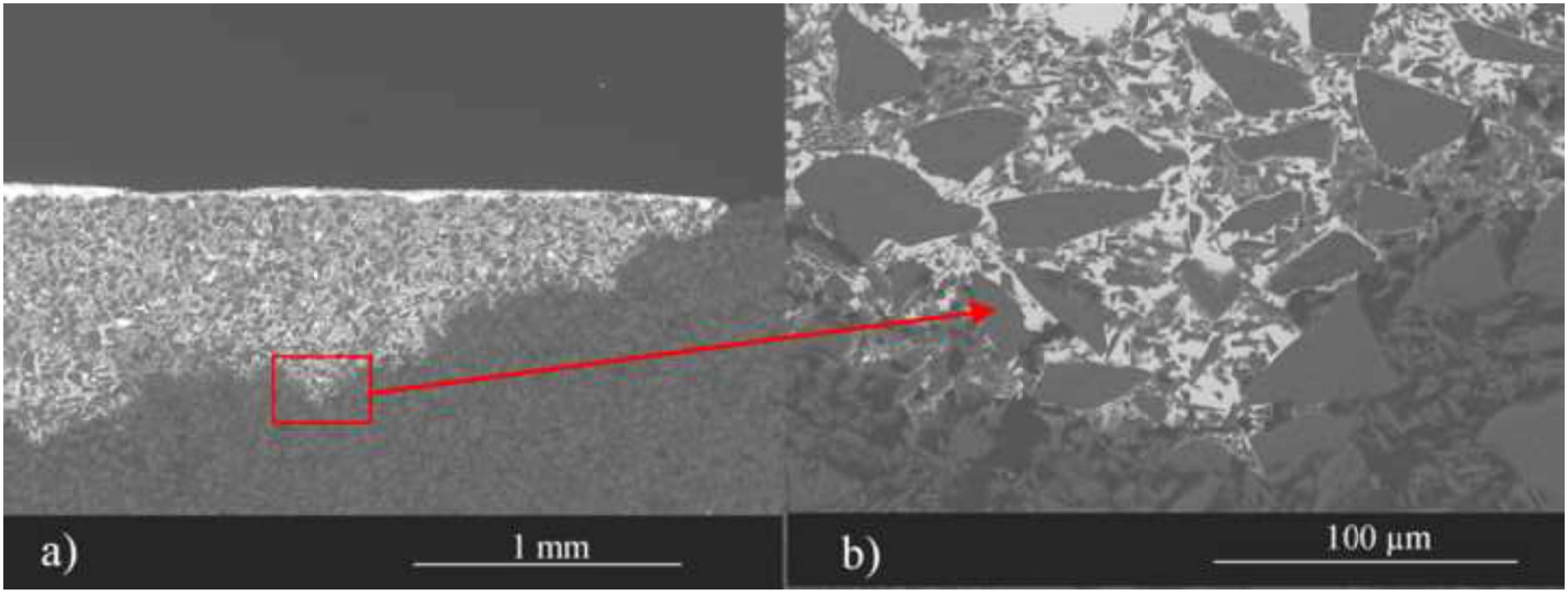

Figure
Click here to download high resolution image

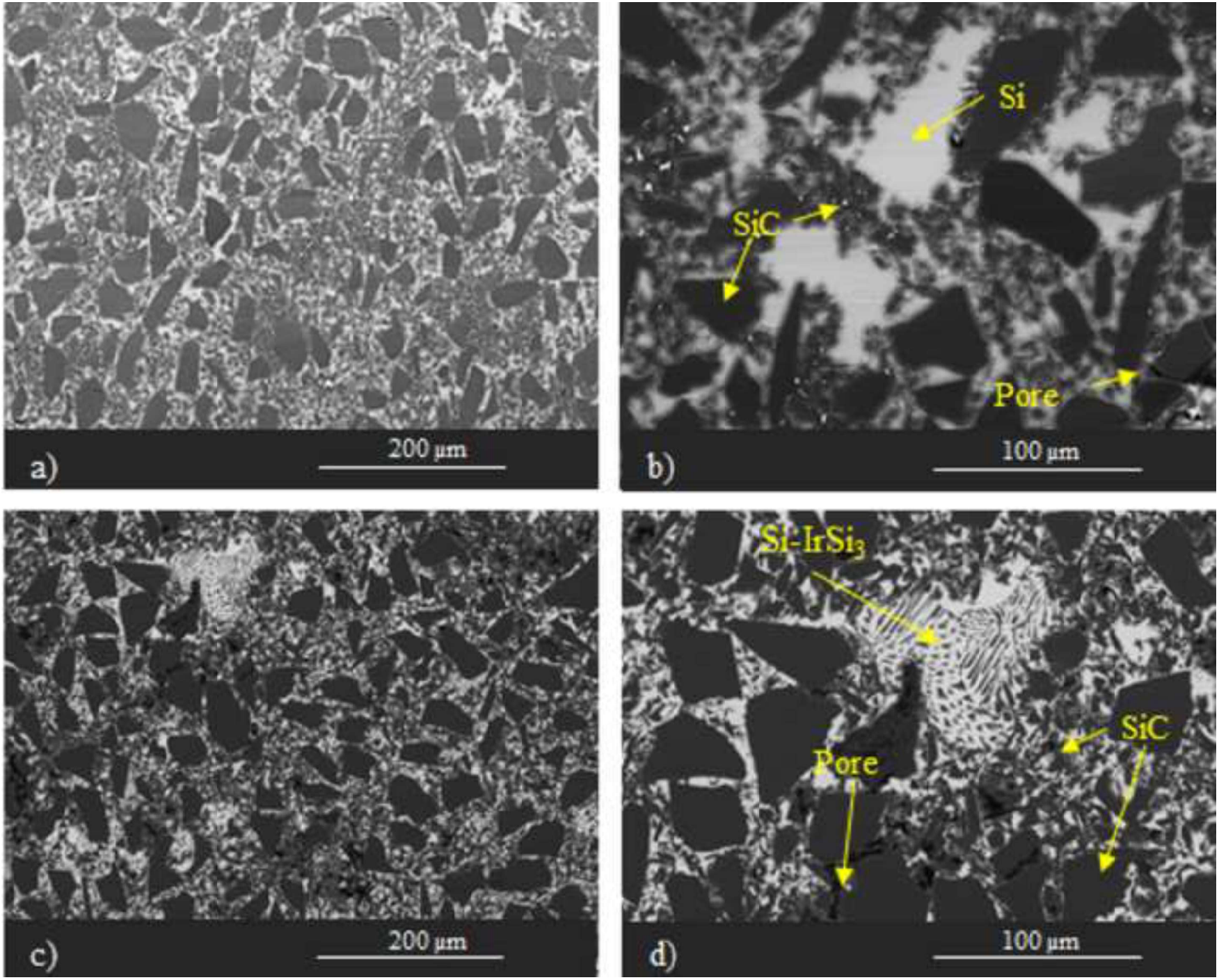

Figure
Click here to download high resolution image

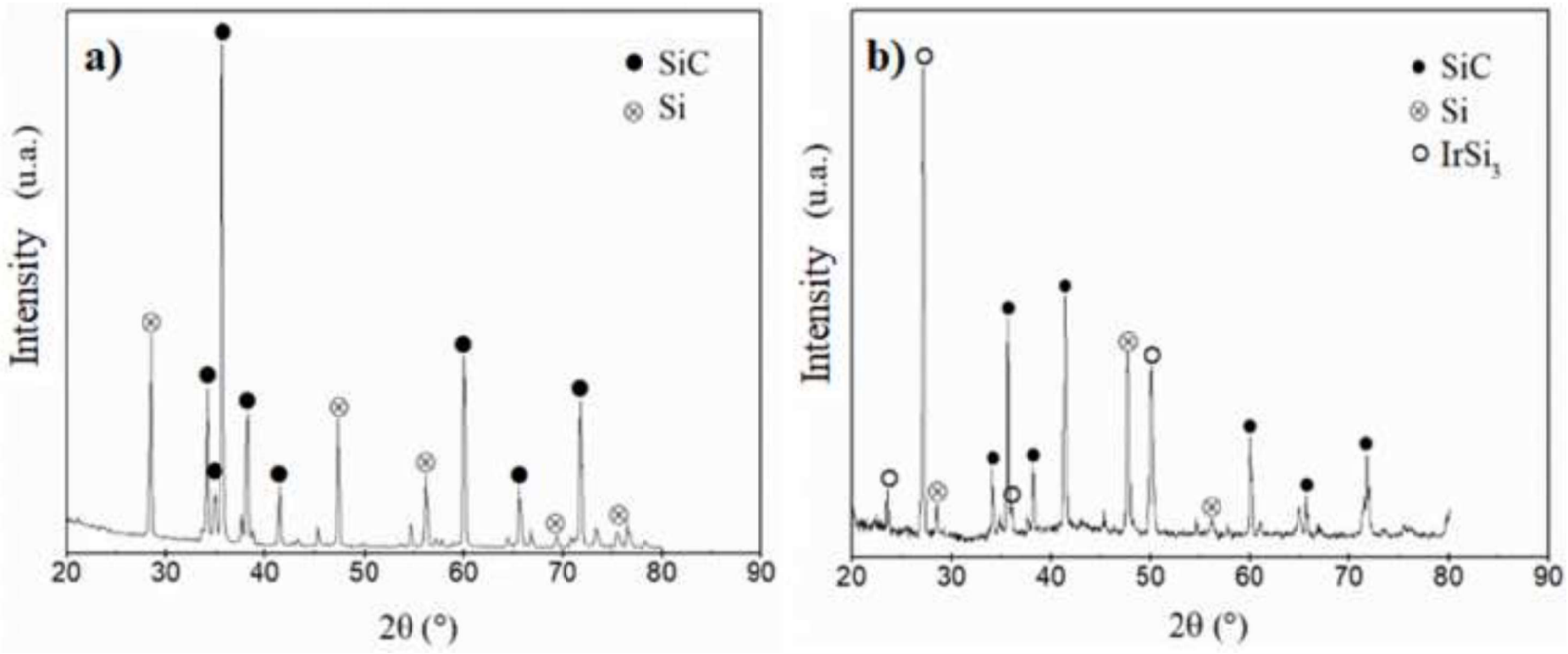

Captions for Figures and Tables

New advanced SiC-based composite materials for use in highly oxidizing environments: synthesis of SiC/$IrSi_3$

Antonio Camarano, Javier Narciso, Donatella Giuranno

Figures

Fig. 1. As received SiC_p-C preform: a) SEM image and b) XRD pattern.

Fig. 2. As-produced Si-62wt%Ir eutectic alloy by arc melting: a) SEM image at the cross-section and b) XRD pattern

Fig. 3. Schematic drawing of the drop with the infiltrated area at the beginning and at the end of the infiltration process [55, 56].

Fig. 4. Evolution of contact angles and drop geometric variables (R-drop base radius and H-drop height) recorded within the infiltration experiments performed on SiC_p-C/Si at T = 1450°C and SiC_p-C/Si-Ir eutectic alloy at T = 1250°C, 1350°C; a) evolution of contact angle, b) evolution of normalized drop height and c) evolution of normalized base radius, d) stages in the evolution of the normalized base radius.

Fig. 5. Scheme of competition between spreading and infiltration and related shape of the drop during infiltration process. U_{spr} = spreading rate and U_{inf} = infiltration rate.

Fig. 6. Images of drop profiles recorded during infiltration experiments performed on SiC_p-C preforms with: a) Si at T = 1450°C, b) Si-Ir eutectic alloy at T = 1350°C and c) Si-Ir eutectic alloy at T = 1250°C.

Fig. 7. Evolution of drop emerging volume (V), infiltrated volume (V_{inf}), and height of infiltration (h_{inf}) for experiments performed on SiC_p-C porous preforms by infiltrating: a) and b) pure Si at T = 1450°C; c) and d) Si-Ir eutectic alloy at T = 1250°C and e) and f) Si-Ir eutectic alloy at T = 1350°C. The linear equation and standard deviation are inserted.

Fig. 8. BSE images of the microstructure after the infiltration of SiC_p-C preforms by pure Si at T = 1450°C: a) global infiltration area and b), c) and d) details of the resulting microstructure at higher magnifications in particular of infiltrated area 1 and 2.

Fig. 9. BSE images of SiC_p-C preform microstructure infiltrated with liquid Si-Ir eutectic alloy at T = 1250°C. a) global microstructure of infiltrated area and b) detail of the infiltration front at higher magnification.

Fig. 10. SEM analyses (retro-scattered electrons) of cross-sectioned composite materials: a) and b) SiC/Si produced at T = 1450°C; and c) and d) SiC/$IrSi_3$ produced at T = 1350°C.

Fig. 11. X-ray diffraction patterns of composite materials: a) SiC/Si produced at T = 1450°C and b) SiC/$IrSi_3$ produced at T = 1350°C

Tab. 1. Characteristics of SiC_p-C Petroceramic preform

Tab. 2. Kinetic parameters (U_{inf}-infiltration and U_{spred}-spreading rates) calculated for infiltration experiments of SiC-C preforms with pure Si and Si-62wt.% Ir alloy, carried out at T = 1450°C, T = 1250°C and T = 1350°C, respectively.